Uncoupling gene expression noise along the central dogma using genome engineered human cell lines

Tyler Quarton[1,2*], Taek Kang[1,2*], Vasileios Papakis[2,3], Khai Nguyen[2,3], Chance Nowak[1,2,3], Yi Li[1,2], Leonidas Bleris[1,2,3]

[1] Bioengineering Department, University of Texas at Dallas, Richardson, Texas, USA

[2] Center for Systems Biology, University of Texas at Dallas, Richardson, Texas, USA

[3] Department of Biological Sciences, University of Texas at Dallas, Richardson, Texas, USA

*Authors contributed equally

Correspondence should be addressed to L.B. (bleris@utdallas.edu)

Supplementary Figures

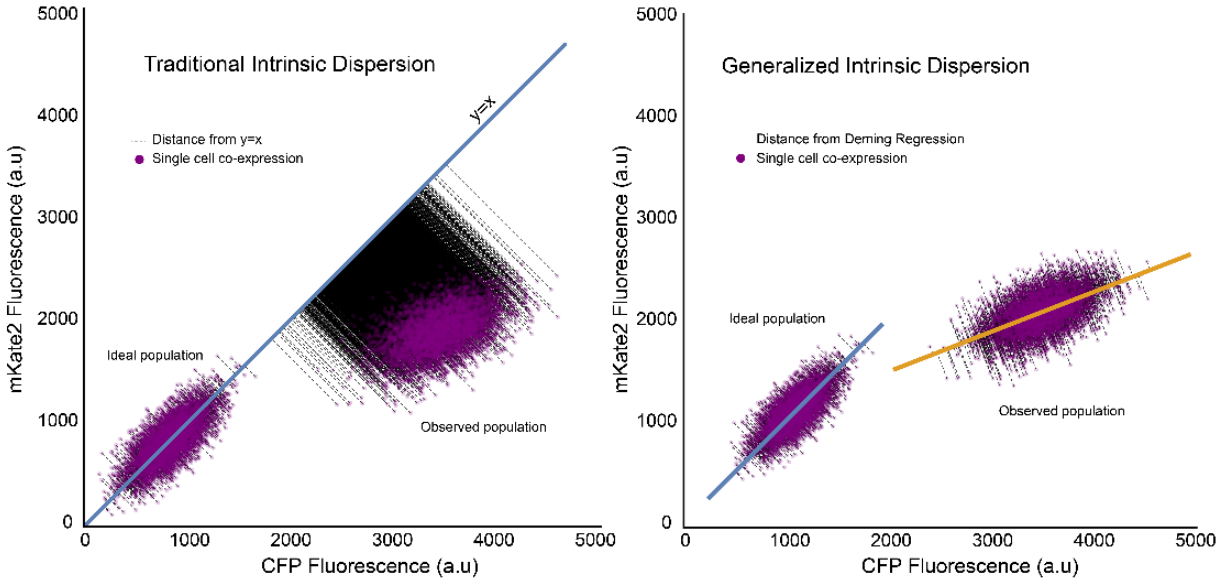

Supplementary Figure 1. Requirements for decomposition of total noise in dual reporter systems. Standard decomposition requires equal mean "Observed population") "Ideal population" (left). In this study, we introduced a decomposition approach that can be applied generally whenever imbalances between reporter expression are present (right).

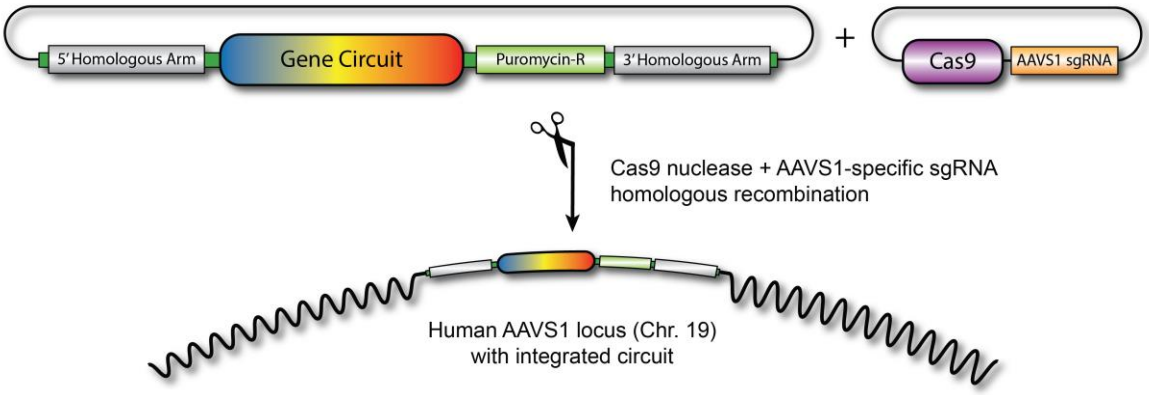

Supplementary Figure 2. Each circuit is stably integrated into the AAVS1 locus using Cas9-mediated homologous recombination.

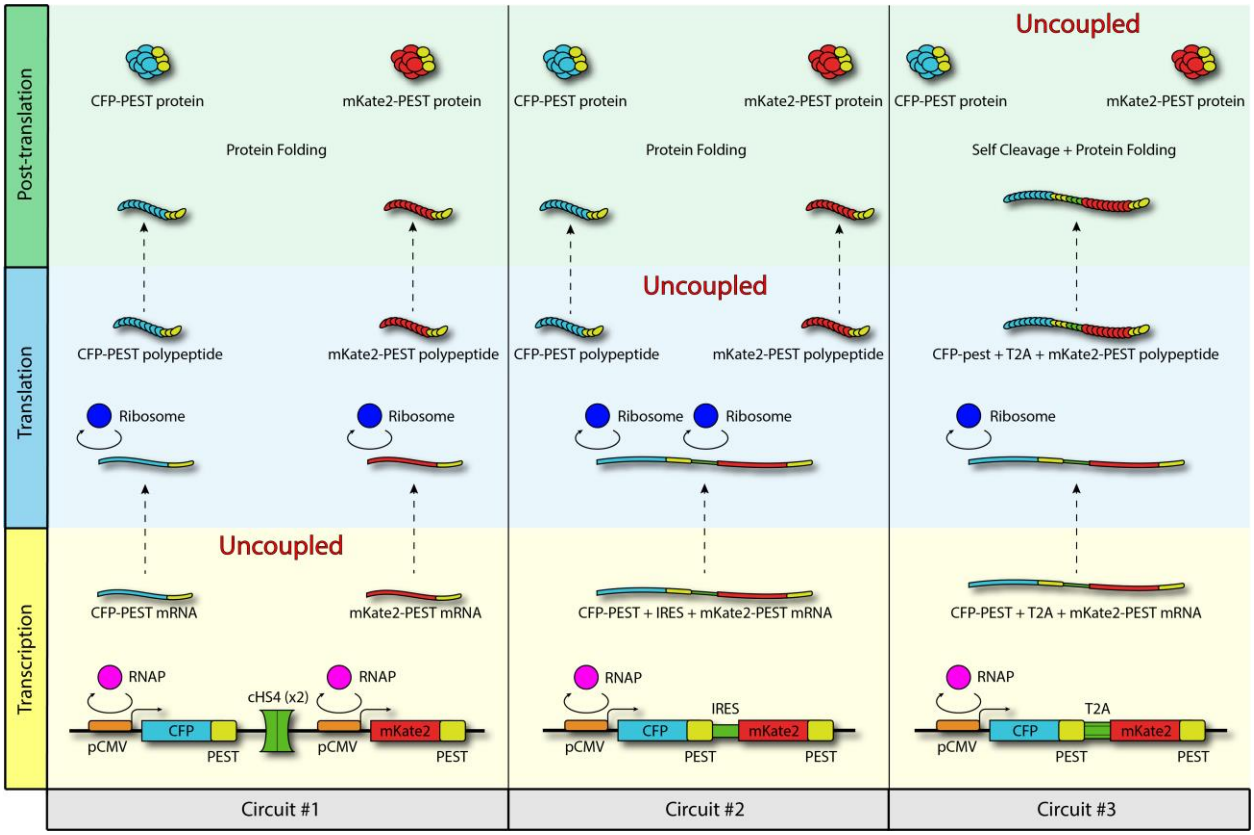

Supplementary Figure 3: Serial uncoupling of noise analyzing circuits. Each circuit uncouples the expression of their respective fluorescent proteins at different production stages. In the transcriptional stage (yellow), the CFP and mKate2 dependent production elements are uncoupled in circuit #1, as two individual genes produce two individual transcripts, and coupled in circuits #2 and #3 as single genes express transcripts that contains both the fluorescent protein's cistrons. In the translation stage (blue), the CFP and mKate2 dependent production persist to be uncoupled for circuit #1, becomes uncoupled for circuit #2, as the internal ribosome entry site allows for a single transcript to produce two polypeptides, and remains coupled for circuit #3. In the post-translational stage (green) circuits #1 and #2 maintain the uncoupled co-expression of CFP and mKate2 while circuit #3 becomes uncoupled through the autocatalytic activity of the T2A element which separates the single transcribed polypeptide into two proteins.

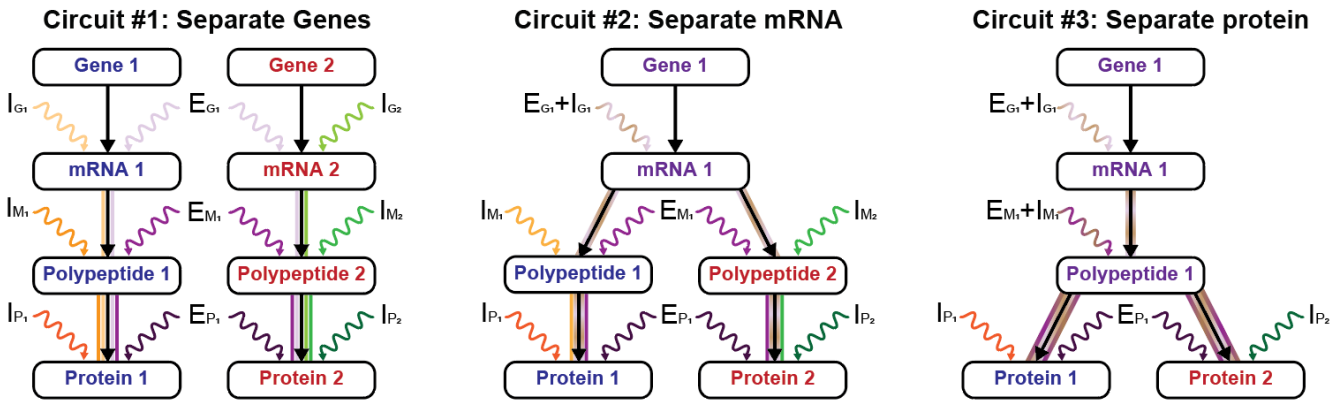

Supplementary Figure 4. Graphical representation of the noise propagation in three circuits. Each process in the central dogma steps is vulnerable to their respective intrinsic and extrinsic sources, and expression of the final gene product (Protein) consists of an accumulation of all preceding steps. If every step is uncoupled (Circuit 1), then the sources of the noise that make up the total noise of the final gene product can be traced back to its origin. Coupling of this process makes a single molecule vulnerable to intrinsic and extrinsic noise simultaneously, making it indistinguishable.

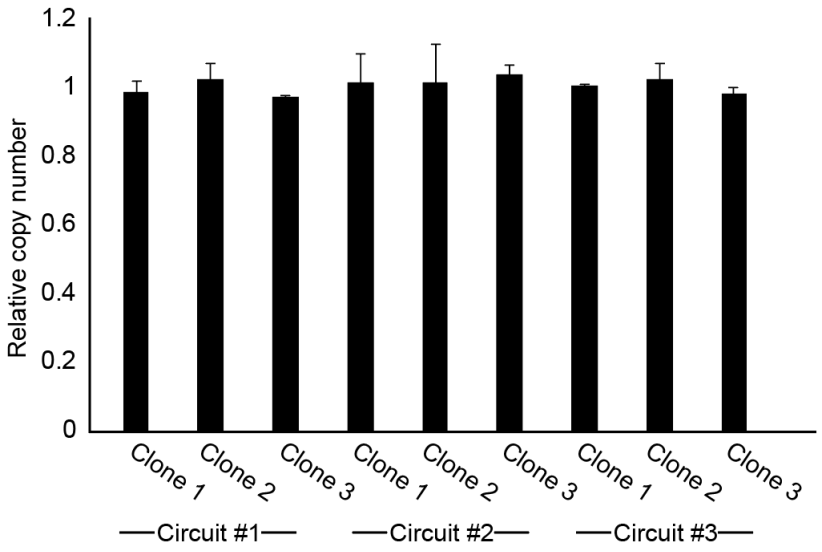

Supplementary Figure 5. Relative copy number analysis of every monoclones.

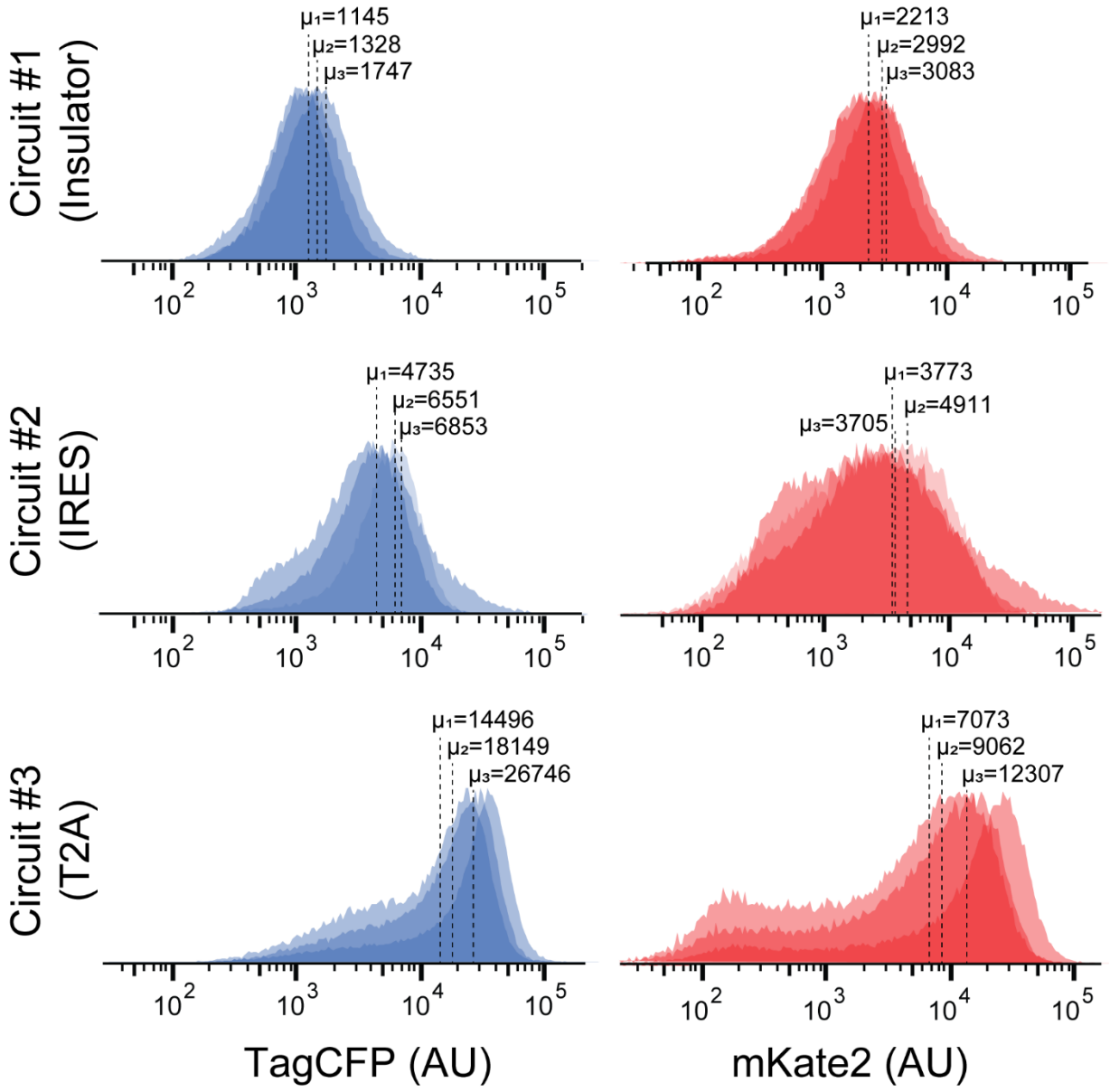

Supplementary Figure 6. Histograms and mean expression values of TagCFP (left) and mKate2 (right) of the monoclonal population.

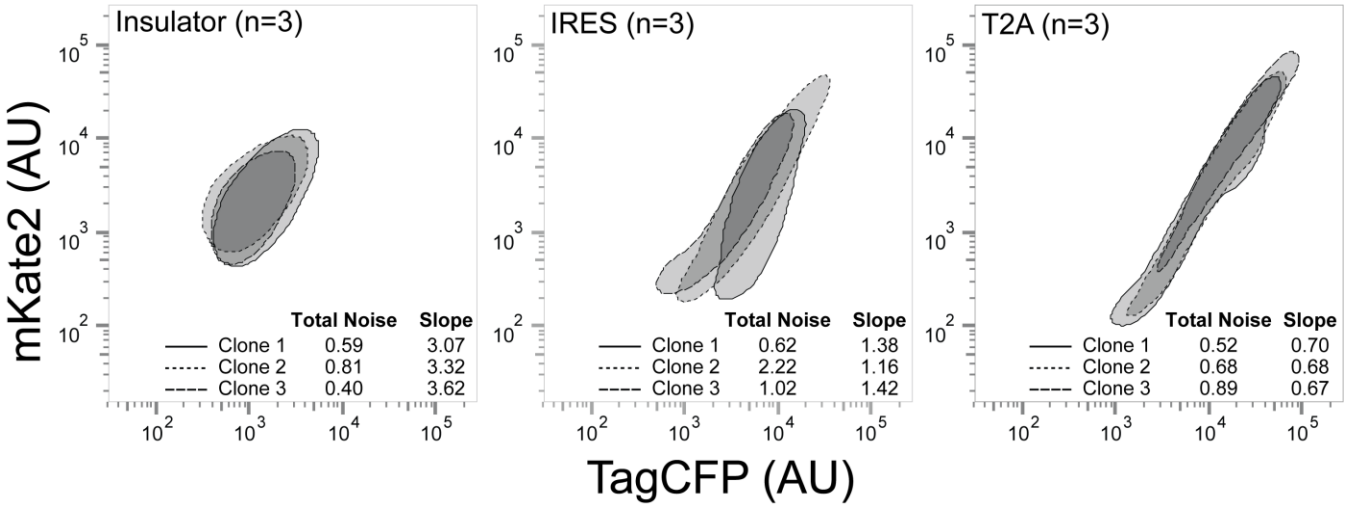

Supplementary Figure 7. Total noise and slope of flow cytometry clouds for each monoclonal population.

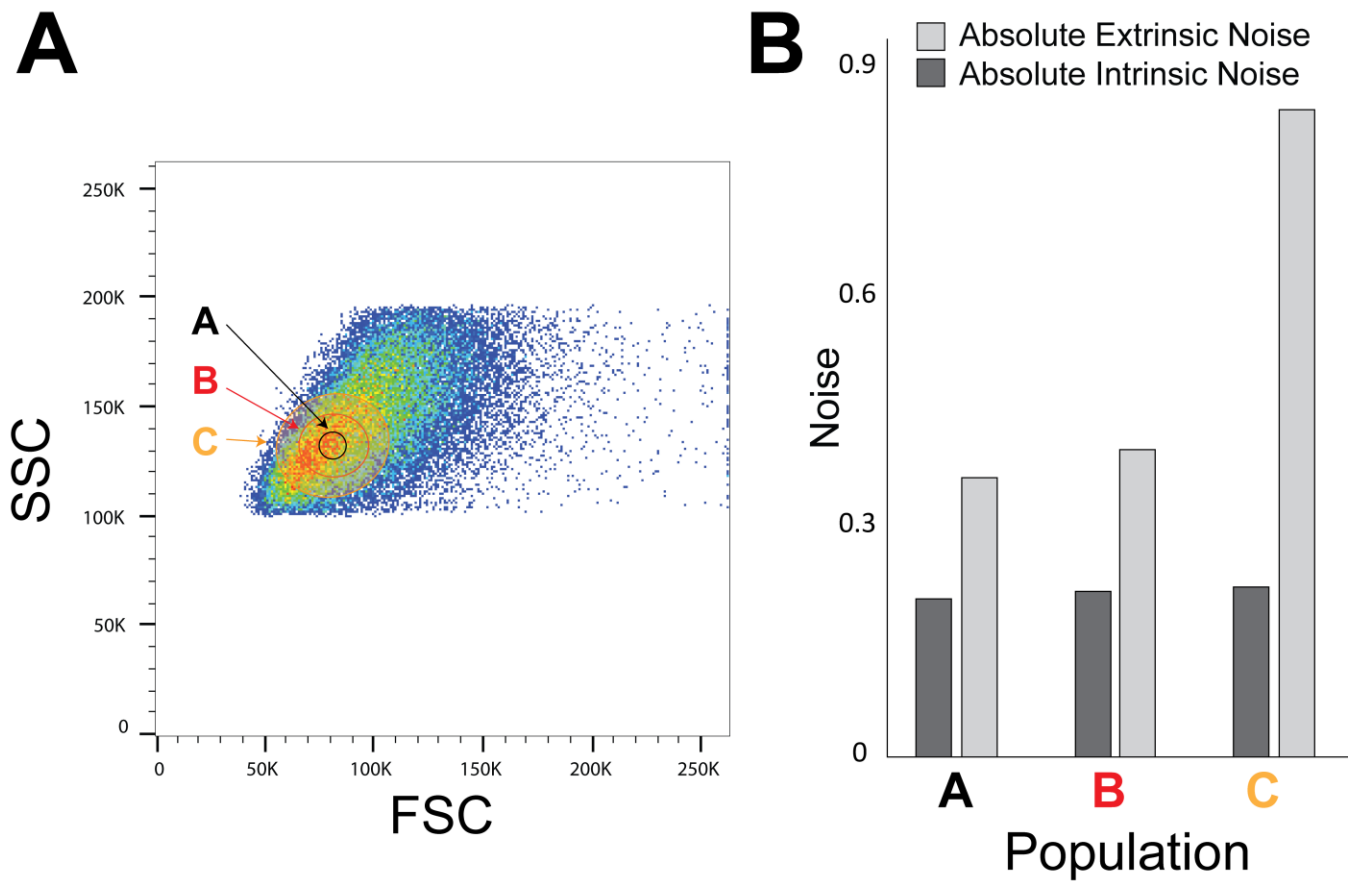

Supplementary Figure 8. Effect of FSC-SSC gate size on decomposed noise.

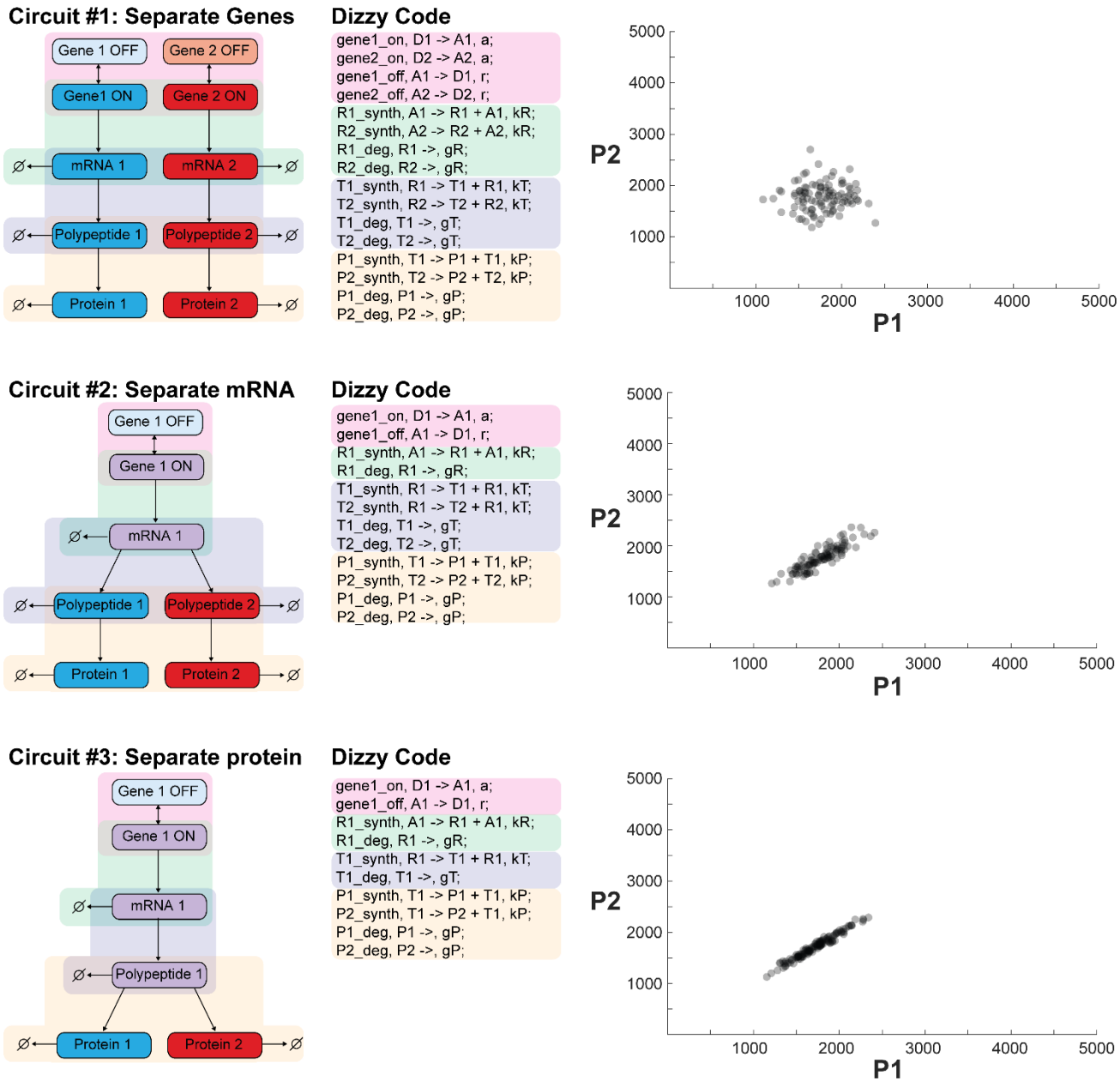

Supplementary Figure 9. Stochastic simulations using Dizzy. The chemical reactions of each circuit were modeled in Dizzy. In this model, the noise of each chemical process determined by the Gillespie stochastic algorithm, which represents intrinsic noise only. Each model was simulated 200 times, and the scatter plot of the results are shown in right.

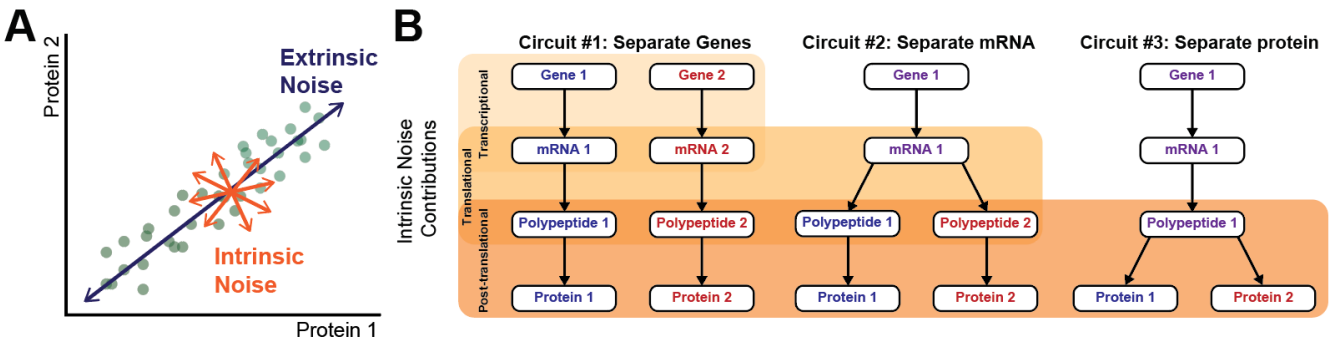

Supplementary Figure 10. A graphical illustration of extrinsic and intrinsic noise spread in a dual fluorescent reporter system. Intrinsic noise contributions that occur at each step in the central dogma process of the synthetic circuits.

EIV Modeling of Extrinsic and Intrinsic Noise in Biological Systems

Consider two variables, X and Y representing two fluorescent proteins, respectively, that are assumed to be observed as

$$x_i = \hat{X} + \delta_i + \theta_i$$
$$y_i = \hat{Y} + \varepsilon_i + \theta_i$$

where $\hat{X}$ and $\hat{Y}$ represents the noiseless true mean of x_i, and y_i respectively, and $\delta_i \sim \mathbf{N}(0, {\sigma_\delta}^2)$, $\varepsilon_i \sim \mathbf{N}(0, {\sigma_\varepsilon}^2)$, and $\theta_i \sim \mathbf{N}(0, {\sigma_\theta}^2)$ are random noise components each sampled independently from their own respective independently distributed normal distributions. We assume that the error parameters are normally distributed such that $E[\delta_i] = E[\varepsilon_i] = E[\theta_i] = 0$ and $Var[\delta_i] = {\sigma_\delta}^2$, $Var[\varepsilon_i] = {\sigma_\varepsilon}^2$ and $Var[\theta_i] = {\sigma_\theta}^2$ for all i.

We interpret the variable specific noise sources, δ_i and ε_i, to be intrinsic sources of noise as these error terms independently obfuscate the true observation of their respective protein. As such, we assume the terms δ_i and ε_i are mutually uncorrelated. Thus,

$$\mathrm{Cov}[\delta_i, \delta_j] = \mathrm{Cov}[\varepsilon_i, \varepsilon_j] = 0, \qquad i \neq j,$$

$$\mathrm{Cov}[\delta_i, \varepsilon_j] = 0, \qquad \forall\, i, j.$$

Furthermore, we interpret the noise source that affects both variables, θ_i, to be an extrinsic source of noise that obfuscates the true observations of both proteins simultaneously while remaining independent of the intrinsic noise sources. Thus,

$$\mathrm{Cov}[\theta_i, \theta_j] = 0, \qquad i \neq j,$$

$$\mathrm{Cov}[\theta_i, \varepsilon_j] = \mathrm{Cov}[\theta_i, \delta_i] = 0 \qquad \forall\, i, j.$$

Derivation of Elowitz's models from our generalized model

The original model of extrinsic and intrinsic noises proposed by Elowitz could be derived from our generalized model when assuming the Demin regression takes the format as:

$$Y = m + k \cdot X$$

where $k = 1$ and m = 0.

Here, the RMS is calculated as:

$$RMS = \sqrt{\frac{1}{n}\sum_{i=1}^{n} dist(\{x_i, y_i\}, y = x)^2}$$

which reduced to

$$RMS = \sqrt{\frac{1}{2n}\sum_{i=1}^{n} (x_i - y_i)^2}$$

or

$$RMS = \sqrt{\frac{\mu_{(x-y)^2}}{2}}$$

where $\mu_{(x-y)^2}$ denotes the mean for $(x-y)^2$.

Finally, the intrinsic noise (η_{int}) is calculated as:

$$\eta_{int}^2 = \frac{RMS^2}{\mu_{\mathbf{X}} \cdot \mu_{\mathbf{Y}}}$$

or

$$\eta_{int}^2 = \frac{\mu_{(x-y)^2}}{2 \cdot \mu_{\mathbf{X}} \cdot \mu_{\mathbf{Y}}}$$

which is identical to the original format proposed by Elowitz.

Supplementary Methods

Plasmid Construction and Integration

For the construction of VP1.1.2 (PCMV-CFP-PEST-T2A-mKate2-PEST), mKate2-PEST was PCR amplified using primers P1.1.1-F and P1.1.1-R and cloned into the AAVS1 donor plasmid (unpublished data) using Eco47III and EcoRV restriction enzyme sites. The reverse primer included an EcoRI restriction enzyme site. The 922bp amplicon and donor plasmid were digested with Eco47III and EcoRI restriction enzymes, then ligated and transformed to give the product VP1.1.1(PCMV-T2A-mKate2-PEST). Using VP1.1.3 (PCMV-CFP-PEST) as template, CFP-PEST was amplified using the forward primer: P1.1.2-F and reverse primer: P1.1.2-R. The forward primer contained a ClaI restriction enzyme site and the reverse an EcoRV restriction enzyme site. The amplicon and VP1.1.1 were digested using ClaI and EcoRV restriction enzymes, then ligated and transformed to give product VP1.1.2 (PCMV-CFP-PEST-T2A-mKate2-PEST).

For the construction of VP1.1.9 (PCMV-CFP-PEST-IRES-mKate2-PEST), CFP-Pest was amplified using CN1.100.6 and forward primer: P1.1.3-F and reverse primer: P1.1.3-R. The forward primer included a ClaI restriction enzyme site and the reverse primer single EcoRI, NsiI and NruI enzyme sites. The amplicon and donor plasmid were digested using ClaI and EcoRI restriction enzymes, then ligated and transformed to give product VP1.1.3 (PCMV-CFP-PEST). In order to remove an unwanted NruI restriction enzyme site upstream of the PCMV promoter, a short region upstream of the promoter was amplified using forward primer: P1.1.4-F and reverse primer: P1.1.4-R. The amplicon and VP1.1.3 were digested with PmlI and ClaI restriction enzymes, then ligated and transformed, giving product VP1.1.4. The IRES sequence was amplified using IRES plasmid (unpublished data) as template and forward primer: P1.1.5-F and reverse primer: P1.1.5-R. The forward primer contained a NruI restriction enzyme site and the reverse primer contained single NsiI and EcoRV restriction enzyme sites. The amplicon and VP1.1.4 were digested using NsiI and NruI, then ligated and transform to give product VP1.1.6. Using B19 (unpublished data) as template, mKate2-PEST was amplified using forward primer: P1.1.6-F and reverse primer: P1.1.6-R. The forward primer contained an EcoRV restriction enzyme site and the reverse primer contained a NsiI restriction enzyme site. The amplicon and VP1.1.6 were digested using EcoRV and NsiI, then ligated and transform to give product VP1.1.9.

For the construction of VP1.1.12 (PCMV-CFP-PEST-PCMV-mKate2-PEST), mKate2-PEST was amplified using Ubc-mKate-PEST (unpublished data) as template with forward primer: P1.1.7-F and

reverse primer: P1.1.7-R. The forward primer contained an Eco47III restriction enzyme site and the reverse primer contained an EcoRI restriction enzyme site. The amplicon and donor plasmids were digested using EcoRI and Eco47III restriction enzymes, then ligated and transformed to give product VP1.1.10 (PCMV-mKate2-PEST). Using VP1.1.10 as template and forward primer: P1.1.8-F and reverse primer: P1.1.8-R, PCMV-mKate2-PEST was amplified. The forward primer contained single NruI and NsiI restriction enzyme sites. The amplicon and VP1.1.9 were digested with NruI and EcoRI restriction enzymes, then ligated and transformed to give product VP1.1.11. VP1.1.11 and K7.35.15 (unpublished data) were digested using NsiI restriction enzyme, then ligated and transformed to give product VP1.1.12 (PCMV-CFP-PEST-PCMV-mKate2-PEST).

Relative transgene copy number

Real-time quantitative PCR (KAPA SYBR FAST qPCR Master Mix Kit, Sigma-Aldrich) has been used as an alternative to Southern blot or fluorescence in situ hybridization for detection of gene copy numbers[1]. The ΔC_t values for each sample were first determined as: $2^{-\Delta C_t} = 2^{-C_t,mKate2} / 2^{-C_t,BRCA1}$, where BRCA1 was used as the reference gene. The relative copy numbers of mKate2 of all stable clones were normalized by using the value of Circuit #3 clone1 as the normalization control. The PCR primers (final concentration 200 nM) are: mKate2 forward primer: 5'- caaaaccttcatcaaccacac-3'; mKate2 reverse primer: 5'- ttcacccctctgatcttgac-3'; BRCA1 forward primer: 5'- gagcgtcccctcacaaataa-3'; and BRCA1 reverse primer: 5'- tgctccgtttggttagttcc-3'. The PCR conditions were as follows: 95 °C for 3 minutes, followed by 40 cycles of 95 °C for 15 seconds and 60 °C for 30 seconds. All genomic DNA samples were extracted using DNeasy Blood and Tissue kit (Qiagen). Three independent DNA samples were obtained for each stable clone, and 50 ng of this harvested genomic DNA was used for PCR. The average copy numbers were calculated as the mean ± SD. For statistical analysis, p-values were calculated using two-tailed t-tests, and p-values larger than 0.05 were determined as no statistical difference.

Primer Table	
P1.1.1-F	CAGTACAGCGCTGATATCGAGGGCAGAGGAAGTCTTCTAACATGCGGTGACG TGGAGGAGAATCCCGGCCCTATGGTGAGCGAGCTGATTAAGGAGA
P1.1.1-R	CAGTACGAATTCTTATCTAGAGACGTTGATCCTGGC
P1.1.2-F	CAGTACATCGATTAGTTATTAATAGTAATCAATTAC
P1.1.2-R	CAGTACGATATCGACGTTGATCCTGGCGCTGGCGCA
P1.1.3-F	CAGTACATCGATTAGTTATTAATAGTAATCAATTAC
P1.1.3-R	CAGTACGAATTCATGCATCAGTACTCGCGATTAGACGTTGATCCTGGCGC
P1.1.4-F	CAGTACCACGTGATGTCCTCTGAGCGGATCCTCCCCG
P1.1.4-R	CAGTACATCGATGGCCTGCAGGGCGAACCGGCCCTGGGAATATAAGGTGGTC CCAG
P1.1.5-F	CAGTACTCGCGAGGGGCCCCTCTCCCTCCCCCCCCC
P1.1.5-R	CAGTACATGCATCAGTACGATATCTGTGGCCATATTATCATCGTGTTT
P1.1.6-F	CAGTACGATATCATGGTGAGCGAGCTGATTAAGGAG
P1.1.6-R	CAGTACATGCATTTATCTAGAGACGTTGATCCTGGC
P1.1.7-F	CAGTACAGCGCTATGGTGAGCGAGCTGATTAAGGAG
P1.1.7-R	CAGTACGAATTCTTATCTAGAGACGTTGATCCTGGC
P1.1.8-F	CAGTACTCGCGAGTCGACAATGGTTACAAATAAAGCAATAGCATCACAAATT TCACAAATAAAGCATTTTTTTCACTGCATGCATTAGTTATTAATAGTAATCAAT TACGGGGT
P1.1.8-R	GAATTCTTATCTAGAGACGTTGATCCCAGTAC

Name	CFP Mean	mKate2 Mean	CFP Variance	mKate2 Variance	CFP mKate Covariance	Slope
ins1_1	1327.521994	2992.390963	1320006.971	5272099.712	1436682.296	3.075926717
ins1_2	1340.537315	3054.377012	1576864.501	5615170.016	1550403.534	2.944303013
ins1_3	1322.179102	2969.645503	1349942.498	4840537.49	1355370.74	2.91807268
ins2_1	1747.614634	3083.711492	2077660.106	10861527.85	2912511.328	3.317284048
ins2_2	1771.798698	3126.151353	2360210.986	11635016.99	3135647.505	3.264229497
ins2_3	1796.388492	3158.423655	2559888.244	12202415.67	3187889.695	3.325424848
ins4_1	1144.63248	2213.437546	536962.2542	2634988.241	627723.4258	3.61853862
ins4_2	1130.760419	2206.412023	560051.1712	2728423.572	655073.1111	3.588680226
ins4_3	1142.388366	2212.262455	553445.9108	2754429.056	634133.4467	3.738344698
ires16_1	6780.203836	5149.915767	58654347.65	105109241.1	70230671.86	1.384012077
ires16_2	6551.885381	4911.770556	54639951.01	93955669.68	63446316.88	1.35673836
ires16_3	6651.635863	4990.545234	56339525.22	94819510.53	64240127.78	1.343389703
ires1_1	6853.653526	3705.137909	14493098.72	18106611.66	12013728.4	1.161618884
ires1_2	7045.158791	4057.253781	15398331.57	20800964.58	13279950.69	1.223877037
ires1_3	6892.321574	3924.806576	14449077.48	18574080.23	12278092.79	1.181981296
ires3_1	4735.463941	3773.578413	13623577.74	24673884.11	15502500.08	1.418025505
t2a11_1	26746.63748	12307.54154	238665198.3	126103565	157161948.7	0.704066884
t2a11_2	27481.62857	13389.31228	249232057.8	139972252.6	170864784.1	0.730131366
t2a11_3	27613.3703	13473.29725	257007060.5	149389183.2	178790814.8	0.743334844
t2a1_1	18149.59557	9062.743357	157713015.9	76843765.65	103025115.9	0.681775776
t2a1_2	18019.1464	8954.53251	159432461.2	77686716.89	103992974.3	0.681422559
t2a1_3	17940.65109	8900.212446	154938118.3	74957336.85	100755541.2	0.67897074
t2a6_1	14496.51558	7073.532986	130681395.7	62939429.52	83547401.02	0.673634957
t2a6_2	14329.89215	6898.789204	129363873.4	60872385.54	81566736.79	0.664702946
t2a6_3	14116.39462	6828.972724	126894097.3	60323632.76	80447954.12	0.668456597
Name	**Extrinsic Noise**	**Intrinsic Noise**	**Total Noise**	**Normalized Ext. Noise**	**Normalized Int. Noise**	**Normalized Total Noise**
ins1_1	0.361660169	0.214712398	0.576372567	0.627476375	0.372523625	1
ins1_2	0.378654567	0.256511915	0.635166482	0.596150109	0.403849891	1
ins1_3	0.345193976	0.225516265	0.570710241	0.604849801	0.395150199	1
ins2_1	0.540440903	0.222613995	0.763054898	0.70825953	0.29174047	1

ins2_2	0.566112646	0.25268455	0.818797196	0.691395438	0.308604562	1
ins2_3	0.561865852	0.282221102	0.844086954	0.665649255	0.334350745	1
ins4_1	0.247762171	0.143470193	0.391232364	0.633286492	0.366713508	1
ins4_2	0.262562416	0.151314066	0.413876482	0.634398009	0.365601991	1
ins4_3	0.250917088	0.151870489	0.402787577	0.622951408	0.377048592	1
ires16_1	2.011332851	0.2265273	2.237860151	0.898775042	0.101224958	1
ires16_2	1.971523932	0.244735703	2.216259636	0.889572639	0.110427361	1
ires16_3	1.935218172	0.256664629	2.191882801	0.882902212	0.117097788	1
ires1_1	0.47309819	0.163466582	0.636564771	0.743205108	0.256794892	1
ires1_2	0.464593899	0.159100926	0.623694825	0.74490581	0.25509419	1
ires1_3	0.453886348	0.150140662	0.60402701	0.751433861	0.248566139	1
ires3_1	0.867532652	0.15059411	1.018126762	0.852087072	0.147912928	1
t2a11_1	0.47742692	0.046931127	0.524358047	0.910497937	0.089502063	1
t2a11_2	0.464356817	0.041353763	0.50571058	0.918226423	0.081773577	1
t2a11_3	0.480564732	0.044311051	0.524875783	0.915578024	0.084421976	1
t2a1_1	0.626349129	0.04014094	0.666490069	0.939772636	0.060227364	1
t2a1_2	0.644505857	0.042284355	0.686790212	0.938431919	0.061568081	1
t2a1_3	0.631001464	0.040996314	0.671997777	0.938993379	0.061006621	1
t2a6_1	0.81476607	0.064932234	0.879698304	0.926188065	0.073811935	1
t2a6_2	0.825082339	0.067307973	0.892390312	0.924575635	0.075424365	1
t2a6_3	0.834518244	0.067913909	0.902432153	0.924743474	0.075256526	1

Supplementary Table 1. Noise Decomposition from Engineered Cell Line. We assume intrinsic noise as the normalized root mean square (RMS) distance from the orthogonal regression line of the two co-expressed reporter proteins. Specific to the reporter proteins used in our constructs, our intrinsic noise quantifies the dispersion of the co-expression of mKate2 and CFP as the RMS distance to an orthogonally regressed line rather than the co-expression line of equality mKate2 = CFP. To enable comparison across different cell lines, the extrinsic and intrinsic noises are normalized to the total noise of 1. For detailed calculation method, see **Generalized noise decomposition** section of the manuscript.

Name	CFP Mean	mKate2 Mean	CFP Variance	mKate2 Variance	CFP mKate Covariance	Slope
Insulator_sim1	7230.337226	7005.560575	33961762.41	32316337.51	25799717.37	0.968567913
Insulator_sim2	7218.431279	7289.006603	33446462.79	33937213.16	25665643.94	1.009584757
Insulator_sim3	7199.445077	7183.007337	33290868.62	32074560.22	24832053.33	0.975756152
Insulator_sim4	7650.031911	7490.094371	35362748.81	34784036.06	26655645.93	0.989163715
Insulator_sim5	7345.106278	7348.152977	36245806.15	36030804.88	28303200.66	0.996189306
Insulator_sim6	7237.984645	7381.060393	33805989.05	34532496.02	25892631.53	1.014128924
Insulator_sim7	7181.086983	7274.303562	30276006.06	34914301.72	24388736.7	1.099695104
Insulator_sim8	7676.384396	7848.637461	37732144.03	38488003.86	28957779.66	1.013120332
Insulator_sim9	7441.496125	7286.290831	32660645.18	33230812.43	24334805.71	1.011773606
Insulator_sim10	7393.687344	7371.732088	33949656.96	37464500.1	27404802.86	1.066227513
IRES_sim1	7281.697153	7068.209898	31261520.73	29539529.87	25061495.07	0.96618544
IRES_sim2	7289.307604	7212.823646	32432217.6	30865528.64	25706303.71	0.969939212
IRES_sim3	7379.650448	7500.122558	32778717.48	35570059.35	28363385.71	1.050457037
IRES_sim4	7256.313857	7328.587163	32653205.01	34732658.11	28553753	1.037107333
IRES_sim5	7322.026644	7311.058536	34629883.67	33588669.19	28889737.75	0.982116134
IRES_sim6	7344.833312	7508.955598	32509916.85	34255798.59	27951660.3	1.031740603
IRES_sim7	7096.174338	7318.428167	33214428.28	33809810.97	28206479	1.010611965
IRES_sim8	6781.008868	6836.386435	27908214.23	28465184.66	23173328.8	1.012085837
IRES_sim9	7155.14384	7023.628051	33395756.2	28340995.47	25113025.41	0.904299689
IRES_sim10	7141.285809	7037.226198	31495017.41	30980649.88	26269257.64	0.990238905
T2A_sim1	6932.728522	7004.17378	32008216.26	32573800.54	29749684.72	1.009555335
T2A_sim2	7177.263763	7241.850179	32865775.24	34609641.49	31007523.44	1.028539478
T2A_sim3	7429.919319	7542.028283	32979024.09	34354056.21	31123866.46	1.02235297
T2A_sim4	7137.481818	7227.977947	29819966.74	31431133.24	28126932.96	1.029076186
T2A_sim5	6842.927506	6875.693756	31521783.35	31973188.53	29083274.78	1.007791935
T2A_sim6	7220.785366	7286.601885	30162932.56	31739418.53	28354599.23	1.028208582
T2A_sim7	7506.883458	7473.53568	39528899.41	38475193.19	36208643.66	0.985537059
T2A_sim8	7094.360413	7048.682602	31888481.01	30630836.15	28393945	0.978073696
T2A_sim9	7370.640112	7399.753129	33864337.8	34569724.43	31701062.99	1.011195034
T2A_sim10	6997.391338	7015.004912	26548777.72	27775833.76	24592941.62	1.025281702

Name	Extrinsic Noise	Intrinsic Noise	Total Noise	Normalized Ext. Noise	Normalized Int. Noise	Normalized Total Noise
Insulator_sim1	0.509346707	0.144636671	0.653983378	0.778837389	0.221162611	1
Insulator_sim2	0.487799101	0.152522886	0.640321986	0.761802829	0.238197171	1
Insulator_sim3	0.480183574	0.151666197	0.631849771	0.759964783	0.240035217	1
Insulator_sim4	0.465198895	0.146880545	0.61207944	0.760030259	0.239969741	1
Insulator_sim5	0.524395888	0.145163431	0.669559319	0.783195563	0.216804437	1
Insulator_sim6	0.484662898	0.154875389	0.639538287	0.757832499	0.242167501	1
Insulator_sim7	0.466882609	0.154992389	0.621874998	0.750766007	0.249233993	1
Insulator_sim8	0.480633764	0.15186649	0.632500255	0.759894973	0.240105027	1
Insulator_sim9	0.448808549	0.158781069	0.607589619	0.738670536	0.261329464	1
Insulator_sim10	0.502800913	0.151290559	0.654091472	0.768701221	0.231298779	1
IRES_sim1	0.486928198	0.103446538	0.590374736	0.824778176	0.175221824	1
IRES_sim2	0.488931528	0.112800166	0.601731694	0.81254076	0.18745924	1
IRES_sim3	0.512452858	0.104369729	0.616822587	0.830794574	0.169205426	1
IRES_sim4	0.536941389	0.096284256	0.633225645	0.847946373	0.152053627	1
IRES_sim5	0.539674669	0.097415959	0.637090628	0.847092462	0.152907538	1
IRES_sim6	0.506811113	0.098229746	0.605040859	0.837647748	0.162352252	1
IRES_sim7	0.543133744	0.102133246	0.64526699	0.8417194	0.1582806	1
IRES_sim8	0.49988201	0.108109515	0.607991526	0.822185819	0.177814181	1
IRES_sim9	0.499711291	0.111998512	0.611709804	0.816909077	0.183090923	1
IRES_sim10	0.522720911	0.098842554	0.621563465	0.840977536	0.159022464	1
T2A_sim1	0.612662446	0.052308122	0.664970568	0.921337689	0.078662311	1
T2A_sim2	0.596566192	0.052291307	0.6488575	0.919410183	0.080589817	1
T2A_sim3	0.555419712	0.045239688	0.6006594	0.924683292	0.075316708	1
T2A_sim4	0.545205897	0.048209037	0.593414933	0.918759987	0.081240013	1
T2A_sim5	0.618137146	0.056606642	0.674743788	0.916106464	0.083893536	1
T2A_sim6	0.538907261	0.04914231	0.588049571	0.916431688	0.083568312	1
T2A_sim7	0.645396299	0.049722328	0.695118628	0.928469291	0.071530709	1
T2A_sim8	0.567811957	0.057168288	0.624980245	0.908527848	0.091472152	1
T2A_sim9	0.581234504	0.046093949	0.627328453	0.926523421	0.073476579	1
T2A_sim10	0.501009933	0.052187468	0.553197401	0.905662124	0.094337876	1

Supplementary Table 2. Noise Decomposition Results from Simulated Datasets. See Supplementary Table 1 for calculation method.